June 15, 1992

A Proposal for

An Experiment to Study the Interference Between Multiple Scattering and Bremsstrahlung (the LPM Effect)

SLAC-Proposal-E146

M. Cavalli-Sforza, L. Kelley, S.R. Klein*
Santa Cruz Institute for Particle Physics
University of California, Santa Cruz, CA 95064

R. Becker-Szendy, G. Niemi, M. Perl, L. Rochester
Stanford Linear Accelerator Center
Stanford, CA 94309

R. Cowan
Laboratory for Nuclear Science
Massachusetts Institute of Technology
Cambridge, MA 02139

P. Bosted
The American University, Washington, D.C., 20016

F. Dietrich, K. VanBibber
Lawrence Livermore National Laboratory
Livermore, CA 94550

* Spokesperson: SPENCER@SCIPP.UCSC.EDU; phone (408) 459-3457.

ABSTRACT

We propose an experiment to test the existence and measure the magnitude of the suppression of bremsstrahlung by multiple scattering, for high energy electrons in dense media, known as the LPM (Landau-Pomeranchuk-Migdal) effect. Because the longitudinal momentum transfer between the electron and the nucleus are small for bremsstrahlung of a low energy photon by a high energy electron, the uncertainty principle requires that the exchange take place over a finite time, or electron path length. During this time, if the electron multiple scatters by a large enough angle, the bremsstrahlung can be disrupted. This effect, predicted in the early 1950's by Landau, Pomeranchuk and Migdal, has never been quantitatively tested. We propose to make an accurate measurement of this effect.

At the same time, we will study the suppression of low energy photon bremsstrahlung due to dielectric suppression, also known as the longitudinal density effect. This occurs when the photon phase shift due to the dielectric constant of the medium ($(\sqrt{\epsilon} - 1) \cdot k$)) becomes large along the length of the medium. This phenomenon occurs for all electron energies, and removes the infrared divergence associated with bremsstrahlung.

The experiment will be performed in End Station A with a fairly simple setup made out of existing equipment. The experiment has been designed to be compatible with the E-142 layout; we request 120 hours of beam time shortly after they run.

1. Introduction

In the early 1950's, a group of Russian theorists led by Landau, Pomeranchuk, Migdal and Feinberg, began studying bremsstrahlung in detail. They realized that, because of the low longitudinal momentum transfer between the nucleus and the electron, bremsstrahlung is not instantaneous, but occurs over a finite formation zone. During this time, external influences can perturb the electron and suppress the photon emission. When this happens, the traditional Bethe-Heitler formulae will fail. The best known example of this is crystal channeling, where photon emission by bremsstrahlung can be enhanced several times. A second case, to be discussed below, is the suppression of low energy photons, when the photon energy becomes comparable to the electron gamma times the plasma frequency of the media. A third example is where multiple scattering disrupts the electron trajectory.

The initial studies of this disruption, by Landau and Pomeranchuk were based on semiclassical arguments.[1] Landau and Pomeranchuk found that multiple scattering can change the $1/\omega_\gamma$ photon spectrum to $1/\sqrt{\omega_\gamma}$. Migdal later used scattering theory to quantify the effect more fully.[2] Because Migdal's derivation is mathematically involved, we will present here a semiclassical derivation of Feinberg and Pomeranchuk.[3]

The classical diagram for bremsstrahlung is presented in Fig. 1a. An electron emits a photon, conserving momentum by exchanging a virtual photon with a nearby nucleus. The transverse momentum exchanged with the nucleus is typically the mass of the electron, m. However, the longitudinal momentum transfer is much smaller,

$$q_{\|} = p_e - p'_e - k = \sqrt{E_e^2 - m^2} - \sqrt{E_e'^2 - m^2} - E_\gamma$$

where p_e, p'_e, E_e, and E'_e are the electron momentum and energy before and after the interaction respectively, and E_γ is the photon energy. For high energy electrons this simplifies to

$$q_{\|} \sim \frac{m^2 E_\gamma}{2E_e(E_e - E_\gamma)} \sim \frac{E_\gamma}{2\gamma^2}$$

where γ is E_e/m, and the latter relationship only holds for $E_\gamma \ll E_e$.

This momentum transfer can be very small. For example, for a 25 GeV electron emitting a 100 MeV photon, $q_{\|}$ is only 0.03 eV/c. Then, by the uncertainty principle, the virtual photon exchange distance is finite, $c\gamma^2/\omega_\gamma$. For a 100 MeV photon from a 25 GeV electron, the formation zone is 2μm long.

The LPM effect comes into play when one considers that the electron must be undisturbed while it traverses this distance. One factor that can disturb the electron, and disrupt the bremsstrahlung, is multiple Coulomb scattering. Semi-classically, if the electron multiple scatters by an angle θ_{MS}, greater than the angle made by the bremsstrahlung photon, $\theta_B \sim$ m/E$_e$, then the bremsstrahlung is suppressed.

One simple parameterization for multiple scattering is[4]

$$\bar{\theta}^2_{MS} = (\frac{E_s}{E_e})^2 \frac{x}{X_0}$$

where E_s is the characteristic energy, $\sqrt{4\pi/\alpha} \cdot m_e = 21$ MeV, x is the scatterer thickness, and X_0 is the radiation length. The above formula is inaccurate for thin media, where single large scatters can contribute significantly to the total scattering; Migdal's analysis considers this in more detail. The LPM effect becomes important when θ_{MS} is larger than θ_B. This occurs for $E_s/E_e\sqrt{x/X_0} > m/E_e$. For a fixed electron energy, suppression becomes significant for photon energies below a certain value, given by

$$E_\gamma < E_e^2/E_{LPM}$$

where all of the constants have been lumped into E$_{LPM}$, given by E$_{LPM}$(eV) = $m^4 X_0/c\hbar E_s^2 = 7.6 \times 10^{12} X_0$(cm), about 2.6 TeV in uranium and 4.2 TeV in lead. For example, suppression becomes significant for 250 MeV photons from a 25 GeV electron in uranium.

Finding the magnitude of the suppression is more involved. For low energy photons, the photon spectrum (multiplied by the energy density) is proportional to $\sqrt{\omega}$, in contrast to the flat Bethe-Heitler spectrum. Beyond that, a more detailed analysis is needed. Migdal used the density of wave states and scattering theory

to derive detailed formulae. Unfortunately, his formulae are recursive and difficult to use. The LPM calculations in this proposal use approximations developed by Stanev and collaborators.[5] The magnitude of the LPM effect for 1 TeV electrons in uranium ($E_e = 1/2\ E_{LPM}$) is shown in Fig. 2.

Aside from the magnitude, two other aspects of the LPM effect are of interest. Neither has been subjected to a careful analysis. First, the LPM effect is angular. Photons emitted at large angles should not be suppressed. Neglecting the LPM effect, the angular distribution of bremsstrahlung photons is

$$P(\theta) = \frac{2(\theta\gamma)^2}{1+(\theta\gamma)^4}$$

Because of this rapid angular dropoff, it is difficult to measure the LPM suppression intensity as a function of angle. However, it may be possible to select a sample of large angle photons which should be free of LPM suppression.

The second aspect is the formation zone length. At 25 GeV, the formation length is $4.8 \times 10^{-4}/E_\gamma(\mathrm{MeV})$ meters. If the target thickness is comparable to this, the LPM effect should begin to disappear, probably as the square root of the thickness. Detailed theoretical calculations have not been done,[6] but it is still an interesting measurement.

An analogous effect occurs for pair creation by a high energy photon. As Fig. 1 shows, the two processes are closely related. In pair creation, the LPM energy threshold is determined by the lepton with the lower energy. Because of this, the pair creation suppression begins at much higher energies than bremsstrahlung suppression.

Although the LPM effect reduces the divergence of the low energy photon production cross section, it does not eliminate it, since dN/dE_γ still grows as $E_\gamma^{-1/2}$. At low photon energies, another effect removes the divergence. For a low enough photon energy, the phase shift due to the effect of the medium ($\sqrt{\epsilon}k$, where k is the photon wave number) can become significant. Then, the contributions to the photon amplitude, $\exp(i(k\cdot x - \omega t))$, from different parts of the electron path through the formation zone can interfere, and photon emission is suppressed.[7] This is sometimes known as the longitudinal density effect, and it is related to the dE/dx

(transverse) density effect discussed by Fermi. The density effect is significant for photon energies less than $\gamma\omega_p$, where ω_p is the plasma frequency. For a given material, this occurs at a fixed E_γ/E_e, and the suppression factor is[8]

$$F_P = (1 + \frac{nr_e\lambda_0^2 E_e^2}{\pi E_\gamma^2})^{-1}$$

where n is the electron density. The density effect becomes important for $E_\gamma/E_e = 10^{-4}$ in lead, for example. The cutoff energies for various materials are shown in Table 1.

Material	E_γ/E_e Cutoff Energy
Carbon	5.5×10^{-5}
Lead	1.1×10^{-4}
Uranium	1.40×10^{-4}
Tungsten	1.43×10^{-4}

Table 1. Cutoff Energies for Dielectric Suppression.

Below these energies, dN/dE_γ goes as $E_\gamma{}^2$, removing the divergence. Although our experiment is not optimized to study this effect, we expect to cover at least one decade (0.5 - 5 MeV) of energy.

In addition to disruption due to multiple scattering and dielectric effects, it is also possible for a magnetic field to suppress the bremsstrahlung. Naively, one would expect that if, over the formation length, the magnetic field bends the electron by an angle larger than the bremsstrahlung emission angle m/E, then suppression can occur. Then the suppression would be comparable in form to the density effect, reducing photon emission below a critical energy, $E_b(eV) = qc\hbar B\gamma^2/m = 5.1 \times 10^{-15} B(G)\gamma^2$, by a factor of $(E_\gamma/E_b)^2$. A more detailed analysis is required; unfortunately, the existing literature on the subject does not appear to give sensible answers.[9]

Before moving on, we note that these formulae fail for very large suppression where higher order corrections become important.

1.1 Physics Interest

The LPM effect is especially interesting because, as John Bell has pointed out, it conflicts with classical electromagnetism, by requiring that total radiation from the electron decrease as the electron energy increases.[10] Bell redid and confirmed Migdals calculations. He argued that the discrepancy between the classical reasoning and the quantum mechanical calculations is resolved by an increased emission of high energy photons, a region where the classical formula is clearly inappropriate. Although doubts have been raised about Bell's calculations,[11] his comments show that the ideas underlying the calculations are of fundamental interest.

Even if the basic ideas are correct, the calculations are complex enough that an experimental check is needed. As will be discussed in chapter 3, we expect to be able to measure the cross sections to 3%, accurate enough for a good check of the calculations. This accuracy is comparable to the expected level of higher order corrections.

1.2 LPM Applications

The LPM effect is relevant in a wide variety of physics applications. In addition to electrons, nuclear analogs of the LPM effect occur during quark hadronization and in stellar interiors, to name two applications. The electron effects described here are also important in a number of areas.

One of the most obvious applications is in calorimeters designed to study TeV particles, for example at SSC, TLC, LHC or a NLC. All of these colliders can produce 1–5 TeV electrons, for which the LPM effect is large. Figure 2 shows one example of this, comparing the LPM and BH cross sections for a 1 TeV electron in uranium. The area under the energy weighted cross section curve is inversely proportional to the radiation length; it increases by about 5% due to the LPM correction. However, the major change is likely to be an increase in granularity of the showers, due to suppression of low energy bremsstrahlung photons which would tend to fill out the showers. This is most likely to manifest itself in electron - hadron separation. For example, electrons may mimic hadronic τ decays. Unfortunately, no calorimeter design studies include the LPM effect; the effect is omitted from both EGS and GEANT, although suppression due to dielectric effects is included in

GEANT, there named the Migdal effect. Analogous effects occur in beamstrahlung, although they do not appear to be significant in currently planned accelerators.[12]

Other applications are more speculative. LPM effects on cosmic ray air showers has been discussed by many authors.[13] In exceedingly high energy (above 10^{18} eV) photon induced air showers showers, the LPM effect increases the graininess of the shower, and changes the shower particle density distribution used in determining total shower energy. Current air shower detectors are insensitive to this effect, but future detectors could be more sensitive. Another potential applications occurs for electromagnetic showers from high energy ν_e as might be produced by active galactic nuclei, and observed by DUMAND.[14]

1.3 Non-Electronic Applications of the LPM Effect

The electronic LPM effect has a number of analogs in nuclear physics. Just as the original LPM effect predicts that photon bremsstrahlung from electrons can be suppressed by multiple Coulomb scattering, its nuclear analog predicts that gluon bremsstrahlung can be suppressed by elastic scattering inside nuclei. Because the nuclear length scales are small, and the elastic scattering is large, the suppression is large, and therefore the cross sections for quark - nuclei interactions are small.

This has been studied by comparing nuclear interactions in various sized nuclei, looking at the extra attenuation in larger nuclei. The EMC data (Fig. 3) indicates that the quark-nucleon inelastic cross section is below 3 mb, far below the typical strong interaction cross sections. Brodsky and collaborators have explained the apparent paradox that a strongly interacting quark interacts only weakly[16] as a suppression of gluon bremsstrahlung by a formation zone phenomenon analogous to the LPM effect. The same physics explains why there is no initial-state interactions which degrade the $q\bar{q}$ c.m. energy in the Drell-Yan process.[17] The nuclear implications of the LPM effect are being pursued by another proposal to the SLAC EPAC.[18]

Although nuclear LPM experiments are very interesting, and the data is very suggestive, all of the analyses are complicated by the strong coupling nature of QCD, which makes interpretation of the data less than straightforward. For this reason, it is important to study the electrodynamic effect, where the experimental

results will be far less ambiguous.

Another system where LPM type suppression appears is in stellar interiors. Although nucleons in a stellar interior are nonrelativistic, the density is very high, and hence collisions are frequent, leading to suppression of nuclear bremsstrahlung. One manifestation of this is that production of neutrinos and axions by bremsstrahlung is suppressed. Since neutrino emission is one mechanism for stellar cooling, solar temperature profiles have been used to put limits on various hypothetical particles such as axions and heavy neutrinos. Recently, Raffelt and Seckel realized that because the nucleon collision rate, Γ_{coll} far exceeds the oscillation frequency of neutrino or axion radiation[19] production of these exotic particles is suppressed and a number of existing limits will need to be reexamined.

1.4 Previous Experiments

A number of previous experiments have attempted to study the LPM effect and dielectric suppression. Except for a 1975 Russian experiment, all of the LPM studies have used cosmic rays. Dielectric suppression has also been studied by several experiments. However, most of the experiments have been focused on studying transition radiation, and only looked at solid radiators as an afterthought.

Most of the cosmic ray experiments were performed during the 1950's, with a few more recent results.[20] One of the better cosmic ray experiments was done by Fowler and collaborators.[21] They studied the depth of pair creation for photons with $E_\gamma > 1$ TeV. Their data (Fig. 4) supports LPM suppression, but their statistics were very limited (47 events).

An experiment at Serpukhov[22] was more successful, but still only produced a qualitative assessment, concluding, "Comparison with theoretical curves shows that this reduction is not less than that predicted by theory. In individual cases (lead and aluminum of thickness 0.05 t_0 and 0.10 t_0), the difference from the theoretical spectrum is somewhat greater." They attribute the difference to systematic errors. To downplay the difference, they presented their data by intensity ratios, including I_{Pb}/I_{Al}, as shown in Figures 5.

The Serpukhov experiment used a 40 GeV electron beam which transited a thin target, was bent by a magnet and disposed of. A NaI crystal was used to detect 20-

80 MeV bremsstrahlung photons. Below 20 MeV, there were many backgrounds, including bremsstrahlung in the air around the target and in the defining scintillation counters, debris from electrons hitting the counter walls, and synchrotron radiation. The experiment was also subject to a large background flux of muons.

Most of the experiments that have reported results on dielectric suppression were done by an Armenian group, using electrons in the 1 GeV range to generate photons of order 100 keV. The experiments were optimized for transition radiation, but they have reported some results with solid targets.[23] Their results, shown in Fig. 6, are at best mixed.

Our proposed experiment follows the general model of the Soviet LPM experiment, but differs in almost all the particulars, to enable us to avoid the backgrounds that caused them trouble, and to measure several additional facets of the LPM effect.

We have recently learned of a tentative proposal to study the LPM effect at Fermilab. The proposal is apparently at an early stage, but hoping to run sometime in 1993.[24] However, the higher energies available at Fermilab are not as helpful as one might expect, because synchrotron radiation grows faster than the LPM or dielectric effects, obscuring the lower energy part of the photon spectrum.

2. The experiment

We propose an experiment in End Station A to study the LPM effect. A block diagram of the experiment is shown in Fig. 7. Many of the experimental elements are chosen because they already exist and are easily obtainable. The most difficult element is the beam, discussed in Section 2.1. The incoming beam hits a thin target (Section 2.2). Bremsstrahlung photons continue 50 meters downstream into a BGO calorimeter (Section 2.3), while a magnet deflects the emerging positrons into a detector array (Section 2.4).

We plan to run the highest energy obtainable in End Station A. Our simulations have assumed a 25 GeV beam. The expected photon cross sections for carbon, lead, and uranium absorbers are shown in Fig. 8. The carbon curve follows the Bethe-Heitler formula except at very low energies, where dielectric suppression is

large. The density effect turn-on for carbon occurs in the 0.5-5.0 MeV range, as as detailed in Fig. 9 (using the previously given formula for F_P).

The energy range of the experiment is set by physics limitations. For photon energies above a few hundred MeV, the LPM and BH curves are very similar. At very low energies, the experiment will be limited by backgrounds. As we discuss in Section 2.6, backgrounds should not be a major problem above 1 MeV. The energy of the incoming electron beam should be high, but at energies close to a TeV higher-order effects would become important.

2.1 The Beam

The experiment requires a beam of approximately one electron or positron per pulse at 25 GeV. Such a beam line existed for many years in End Station B. It is Beam Line 19, a secondary positron beam which was last used for a channeling experiment in the early 1980's. Unfortunately it is now in disrepair and it is estimated that \$200-400K would be required to make it operational again. It is also not known what problems might be encountered in bringing the primary electron beam through the B-line in the Beam Switchyard (BSY).

However, by adding a thin positron target near the beginning of the BSY, the A-line can be used as a low intensity, secondary positron beam, just as was done in End Station B. A good location for the target is in the pulse magnet string, as shown in Fig. 10. Figure 11 shows an EGS calculation of the yield of 25 GeV e^+ from a 30 GeV e^- beam as a function of target thickness. The lower curve is approximately the acceptance of the A-line from a target position at the end of the BSY pulse magnet string. For a 2% X_0 target, there are 2×10^{-7} e^+/e^-. A long pulse primary beam of modest intensity - 10^9 to 10^{10} e^- per pulse - directed onto the target will give more than enough 25 GeV positrons into End Station A. The positron intensity can be adjusted with the A-line energy slit (SL-10) and a variable jaw collimator (C-12) just as was done in Beam Line 19. With the production target located between pulse magnets 4 and 5, the low power, primary electron beam can be directed onto the Tune-up Dump (D-10).

The positrons generated by this target have been tracked into end station A using TURTLE, a beam transport program. For a beamline acceptance of $\Delta E/E =$

$\pm 0.2\%$, TURTLE found σ_x = 2.2 mm, σ_y = 1.6 mm, σ_θ = 0.035 mrad, and σ_ϕ= 0.10 mrad at the target in End Station A.

To simplify the beam tuning process, it may be necessary to install one or two removable scintillator paddles into the A-line.

2.2 The Target

We plan to take data with 4 target materials: carbon, lead, uranium and tungsten. The first three targets display a good mix of LPM turn on energies. Tungsten is interesting because it has a radiation length similar to uranium, but a significantly lower Z, providing an additional test of the LPM theory. For the initial phase of the experiment, the targets will be a uniform number of radiation lengths thick. The optimal choice of thickness is still under study, but 0.05 and 0.1 X_0 are reasonable choices. The LPM and dielectric suppressions remove the infrared divergence in the Bethe-Heitler spectrum. Over the entire photon energy range, there are about 8.7, 9.3 and 11.9 photons emitted per radiation length in carbon, lead and uranium respectively. The spectrum peaks at a few MeV, where the dielectric suppression disappears. At 1 photon/positron, 2 photon pileup will be nonnegligible. However, because this experiment is focused on the low energy (below 300 MeV) part of the photon spectrum, the problem is less important. This is because, if two or more photons are produced, the chances is large that the sum of their energies will be higher, out of the region of interest. This has been studied by Monte Carlo simulation, as shown in Fig. 12 for a 0.1 X_0 thickness radiator. The curve showing total event (calorimeter) energy is much lower than the curve showing individual photon energies, because often a low energy photon is combined with a higher energy photon, pushing it off the plot. However, the shape of the two curves are very similar, and the correction can be determined by Monte Carlo.

After good bremsstrahlung spectra are collected with uniform thickness targets, we plan to study the effects of varying target thickness. The reason for this is that, as the target thickness becomes comparable to the LPM formation zone length, the LPM effect should disappear.

We plan to use a 7 position remotely operable target holder, for example the one used recently by Meyerhof.[25] The area upstream of the calorimeter will be kept

in vacuum, to avoid bremsstrahlung from air. This can be done almost entirely with existing vacuum plumbing.

2.3 CALORIMETER

To measure the photon energy, we will use a BGO calorimeter built by the UCSC group.[26] As Fig. 13 shows, the calorimeter consists of 45 BGO crystals, each 2 cm square by 20 cm (18 X_0)deep, arranged in a 7 by 7 array without the 4 corners. Each crystal is read out by it's own PMT. The calorimeter was exposed to 40–100 MeV electrons at the Monterey Naval Postgraduate School Linac and to 1–8 GeV electrons at SLAC. The 100 MeV data is shown in Fig. 14. The energy resolution as a function of energy is shown in Fig. 15. Energy resolution full width at half maximum improves from 8% at 40 MeV to 6% measured at 70 and 100 MeV. At 8 GeV, it reaches 4.4%.

The photon angular resolution depends on the calorimeter – target separation and the calorimeter position resolution. The position resolution is less well known, but if the photons are merely localized to a single 2 cm crystal, the resolution is $\sigma \sim 2\text{cm}/\sqrt{12} = 0.6\text{cm}$. This is already better than needed; we expect to use energy sharing among the crystals to do somewhat better. To maximize the angular resolution, we will place the calorimeter far downstream. The optimal location appears to be the back of the end station, allowing a 50 meter flight path, for a 0.1 mr angular resolution, less than the 0.2 mr from the electron multiple scattering (assuming that the photon is emitted in the middle of a 0.1 X_0 thick target) and comparable to the 0.1 mr beam divergence.

We will place a thin scintillator immediately in front of the calorimeter. This will be used to detect upstream pair conversions and other charged particle backgrounds.

Because the calorimeter has not been used for several years, it will be necessary to recommission and recalibrate it. Since the linearity is well known, much of this can be done with radioactive sources.

2.4 Magnet and Wire Chambers

To bend the electrons away from the calorimeter, we plan to use an 18D72 magnet mounted where the E-142 Moller spectrometer bend magnet is currently mounted. Most likely, this will be the current Moller magnet with the septum removed (this should be a simple change). If problems occur we will use a different 18D72.

We plan to use a set of wire chambers built to fit on the 8 GeV/c spectrometer in End Station A.[27] There are a total of 12 chambers, 6 p chambers and 6 θ chambers, with a 35 by 93 cm active area, with wires on a 2 mm pitch. In the θ chambers, the wires are ganged in groups of 2, giving a 4 mm accuracy. The set includes power supplies, gas system, chamber and readout electronics, and software, allowing for easy CAMAC readout and analysis. A blowup of the chamber construction, together with a plot of chamber efficiency are shown in Fig. 16. Behind the wire chambers, we will place a slab of scintillator. With fast timing electronics and perhaps dE/dx measurement, this scintillator will allow us to count passing electrons.

If the wire chambers are 15 meters downstream of the magnet, just forward of the E-142 polarized target, the angular resolution is (2 mm / 15 meters) $/\sqrt{12}$ = 0.04 mr, better than the 0.3 mr electron multiple scattering in the target, which is itself less than the multiple scattering from the electrons exiting the beampipe. By placing the chambers upstream of the E-142 target, our setup is simplified.

Because of the geometry, with the target close to the magnet, it is not possible use tracking to separate the effects of multiple scattering and electron momentum. So, the limiting factor in the electron energy resolution is multiple scattering in the target, giving $\Delta p/p$ = 0.3 mr/50 mr = 0.6%, or 150 MeV at 25 GeV. This will provide a useful constraint in rejecting a variety of backgrounds, but will not help in determining the photon energy.

2.5 ELECTRONICS AND DAQ

The data acquisition requirements are small on the scale of current experiments. A block diagram of the electronics is shown in Fig. 17. The system uses commercial NIM electronics for the trigger, CAMAC for data acquisition, and the ESA computer system, with the data being stored on 8mm tape. As a less attractive alternative, we can use a Macintosh-based system which exists at UCSC.

Due to the low rate of incoming particles (typically one interaction per beam pulse, at 120 pps), the trigger system is very simple. The accelerator beam gate (T0) is used as a timing reference. The trigger is formed from an "or" of the calorimeter signals (that could also be replaced by an energy-sum trigger), if necessary qualified by a scintillator mounted behind the wire chamber. That requires a set of discriminators and a multiplicity-logic-unit for the calorimeter outputs.

The 45 channels of the BGO calorimeter require ADC readout, with a usable dynamic range from 1 MeV (about 100 keV least count) to several hundred MeV, and with enough resolution to be able to detect showers being shared by neighboring crystals (for improved position resolution). That requires digitizing each PMT signal with two ADCs with different gains to give an adequate dynamic range. Eight LeCroy 2249 ADC modules are needed, along with PMT signal distribution fanouts, discriminators (for the trigger and TDCs) and amplifiers (possibly LeCroy 612 PMT amps) and TDCs (to separate in time and out of time signals).

The drift chamber has its own readout system, which uses 2 slots in the CAMAC crate, and provides the addresses of the wires which have been hit. The gate signal, for the drift chamber readout as well as for the calorimeter ADC and TDC, is provided by the beam gate, with suitable delay and gate width.

To discriminate between one and more positrons per bunch, we will use a piece of scintillator with fast readout. Since the average rate of positrons is $1/1.6\mu$sec, a 15 nsec two pulse resolution, provides a missed dual electron rate less than 1%. This can be further reduced by using the wire chamber information and dE/dx data from the scintillator.

All the data acquisition electronics fits into a single CAMAC crate, with a NIM bin dedicated to discriminators and trigger logic. There are two options for

readout. The VAX-based E142 data acquisition system can trivially be modified to read out the CAMAC crate, and write the data to an 8mm tape. The software and hardware (VAX 3400) both exist, and being designed for the data rate and complexity of E142 they are rather overkill for this task. If we want to also analyze a part of the data online, another VAX (connected via DECnet) is required. We can either use one of the ESA machines, or a UCSC VAXstation 3100. The software to transfer the data and allow online analysis is being developed by the E142 group for their purposes, and can be modified with small effort for this experiment.

The second option is to employ a Macintosh IIci computer (provided by UCSC) for the readout, using the Micron/MacVee crate controller and interface. The data rate of this experiment (about 120 events per second, with about 150 channels of CAMAC data) will be at the limits of what this setup can handle, and online event filtering (for example energy cuts on the calorimeter) may be required.

The DAQ electronics is all already in hand. The electronics is available at UCSC or SLAC. The computer will either be the E142 system, or a Macintosh from the UCSC group. No purchases of major equipment items will be required for this experiment.

2.6 Backgrounds

Most of the backgrounds that affected the Soviet experiment are avoidable. We plan to run our beams in vacuum, removing bremsstrahlung from air in the beam line. Since our target is very simple, this is not difficult. Also, we will avoid scintillators upstream of the target where bremsstrahlung from them can be seen by the calorimeter. If necessary, we will use a movable scintillation detector for beam tuning. With these measures, we expect the major sources of background to be multiphoton pileup (discussed in Section 2.3), synchrotron radiation and transition radiation.

The average synchrotron radiation from the spectrometer magnet which will hit the calorimeter (opening aperture is 7.5 cm half width 50 meters downstream) is 200 keV per positron. Because the critical energy is large, 1.6 MeV, the number of photons is small and the pulse to pulse variation large. In addition to the spectrometer magnet, there will also be a small contribution from the final A

line bend magnet, estimated at 44 keV/positron, with a 1.1 MeV critical energy. The photons will form a narrow band from the calorimeter center running down (spectrometer magnet) or sideways (A line bend magnet). Roughly 2/3 of the synchrotron radiation can be rejected using the position resolution of the calorimeter. Beyond that, we will collect a no-target spectrum which can be subtracted from the bremsstrahlung spectra to remove this background.

As was previously mentioned, transition radiation and the density effect have similar physical origins, and hence similar length and energy scales. For targets thicker than the formation zone size, $\gamma^2 c/\omega_\gamma$ at the photon critical energy, $\gamma\omega_p$, there is little interaction between the two sides of the target, and the transition radiation is easy to calculate. The transition radiation intensity is then about 7 keV per interface, or 14 keV. Again, the average photon energy is large, several hundred keV, with occasional photons ranging up to a few MeV. The thick target transition radiation can be measured by comparing photon energy spectra from like Z targets with different thicknesses.

In summary, the major background sources are only large below 1 MeV. If they can be understood at the 10% level, then their contribution to the overall systematic error for the LPM effect should be less than a few percent. For the longitudinal density effect studies, the photon energies are lower, and hence the backgrounds will be higher, but their contribution to the systematic error will be at most at a 10-20% level.

2.7 Experimental Program

Our first priority is to get a clean, high statistics photon energy spectrum for the four materials discussed above, simultaneously collecting data to study the LPM effect and dielectric suppression. The number of events that we need is driven by the low energy end of the photon spectrum, where the yield is far below the Bethe Heitler spectrum. For example, the yield of 400 keV photons from carbon is only 10% of the BH prediction, while in uranium it is only about 2%. This proposal will use 400 keV photons from carbon as a basis for run length calculations.

We aim to run at close to 1 event/pulse. Assuming a Poisson distribution, at an average of 1 e^+/pulse, 36% of the pulses will contain exactly 1 e^+. We will also

accept the first positron in multiple positron events where the 2nd positron comes more than 300 nsec (the calorimeter response time) after the first one, increasing the fraction of usable pulses to about 60%,[28] or about 2.6×10^5 events/hour at 120 pps. For the Bethe-Heitler 1/E spectrum, 1% of all photons will fall in a bin of width $\Delta E/E = 0.1$. A 0.1 X_0 thick target with no LPM suppression yields 2.6×10^3 counts/hour in a 10% ΔE/E bin. For the carbon example, the count rate is 260 photons/hour in a 10% of E bin. Because of the multiphoton pileup discussed in Section 2.2, the effect count rate at the energies of interest is reduced by about 50%. So, to achieve a 3% statistical accuracy takes 10 hours. A 3% statistical accuracy is selected as a goal because we expect other systematic effects, such as calorimeter resolution, to become significant at this level.

Because backgrounds are significant at these energies, and must be subtracted statistically, the overall statistical error will be larger. The synchrotron radiation can be measured by running with no target. To match the statistics, an equal amount of running time is required. The transition radiation is more complicated. To study it, we will run with two different target thicknesses and subtract them. As long as the targets are thicker than the formation length, so the two interfaces do not interfere, the subtraction is valid. So, we will need to run with 9 targets, two thicknesses of four targets (carbon, lead, uranium, tungsten) plus an empty target holder, for a total of 90 hours.

An alternate consideration in deciding running time is the desire to get a sample of large angle bremsstrahlung photons. Our ability to find 'off axis' photons is limited by the calorimeter position resolution, with a smaller contribution from the beam divergence. As discussed above, the resolution limiting factor is multiple scattering in the target, 0.2 mr. Since multiple scattering is proportional to $\sqrt{\text{thickness}}$, it is hard to reduce this by using a thinner target. To get a clean separation, it will probably be necessary to go to 4σ, or 0.8 mr. There, $\theta\gamma$ is 40 and the photon intensity is down a factor of 800. Combining all of the targets and photons where the LPM suppression is larger than 50%, but above the dielectric suppression region (where different angular effects appear) gives a signal of about 20,000 usable photons. However, without actual data, it is impossible to be confident about possible non-gaussian resolution tails which could produce large backgrounds. So, although the numbers are positive, we have relegated this

potentially very interesting study to a secondary consideration.

The second phase of the experiment will use foils with thicknesses comparable to the length of the formation zone. For this, a single material will suffice. Because the formation zone length depends on the photon energy, choosing thicknesses is not straightforward. We have chosen to run at five thicknesses, likely 1 mm, 0.5 mm, 0.25 mm, 0.12 mm and 0.06 mm, corresponding to one formation zone at photon energies of 0.5, 1.0, 2.0, 4.0 and 8.0 MeV. The data analysis for this is complicated because the bremsstrahlung photon intensity drops, while the transition radiation and synchrotron radiation backgrounds remain the same. While we will compensate for the overall signal level by increasing the number of positrons per pulse, the signal to noise ratio will still drop. Because of the low energies of interest, accumulating statistics will be slower. Given that there are no thin target calculations, our run time request is somewhat arbitrary; for consistency with our first phase, we request 10 hours of running per target thickness. Since two of the thickness are identical to those used in the first phase of the experiment, this phase only requires 30 additional hours of beam time.

In addition to running time, it will take some beam time to set up and tune the positron beam and our detector; we estimate this will take 5 days. The most difficult problem will be (re)commissioning the beam; we expect this to take the majority of the time. If we run immediately after E-142, when the A line operational, this time can be reduced by 1-2 days.

Type	N_{targ}	% Acc.	Run Time
Setup	-	-	5 days
Normal	5	3%	90 hours
Thin	5	10%	30 hours

Table 2. Requested Running Time.

We would like to run late in 1992, after experiment E-142. As most of the experimental apparatus already exists, we require relatively little advanced preparation. The calorimeter needs to be recommissioned, but this should take less than a month. The biggest job is designing the positron target and associated beam transport; this should take a few months, so we can easily be ready by the winter.

It will take 1 week to set up our apparatus in End Station A after E-142. We have laid out our apparatus to minimize conflict with the E-142 setup, allowing much of the installation to precede E-142 datataking, so that changeover can be quick. The major changes will involve flipping the polarity of the A-line to transport positrons, adjusting the vacuum piping to accommodate our experiment, ensuring an uninterrupted photon transport through the E-142 target area and installing our calorimeter. Our target holder and wire chamber can be installed beforehand.

There is no reason not to run soon. We note that this would give us a large lead over the proposed Fermilab experiment mentioned above, and would ensure that the measurement is done first at SLAC.

2.8 Institutional Responsibilities

In general, most of the experimental components are being handled by the institutions that built them. UCSC is responsible for the calorimeter, target, and overall coordination. SLAC group C is responsible for the electronics. SLAC Group E will provide technical support. American University will handle the wire chambers and LLNL will be in charge of the mechanical design and layout in ESA. MIT will oversee the computers and software. The Experimental Facilities Department at SLAC will be responsible for the positron target design and will participate in commissioning the beam.

3. Conclusions

The LPM effect was first predicted nearly 40 years ago; it is time for a good experimental measurement. When it was first predicted, the energies were far beyond the reach of any planned accelerators; 40 years later it is becoming a significant issue in many areas of physics.

The experiment is not that difficult and SLAC is the best place for it; it's time to do it.

Acknowledgements

Many people contributed ideas to this proposal. Lew Keller, Roger Gearhart and the SLAC EFD group provided enormous assistance in designing the beam line. Don Coyne provided encouragement and numerous helpful suggestions. Don Briggs and Mark Petree provided useful advice about the electronics and data acquisition.

REFERENCES

[1] L. D. Landau and I.J. Pomeranchuk, Dokl. Akad. Nauk. SSSR **92**, 535 (1953); **92**, 735 (1953). These two papers are available in English in L. Landau, *The Collected Papers of L.D. Landau*, Pergamon Press, 1965.

[2] A.B. Migdal, Phys. Rev. **103**, 1811 (1956).

[3] E.L. Feinberg and I. Pomeranchuk, Nuovo Cimento, Supplement to Vol **3**, 652 (1956).

[4] See, for example, R.M. Sternheimer, in *Methods of Experimental Physics, Vol 5, Part A: Nuclear Physics*, ed. L. Yuan and C.S. Wu, Academic Press, 1961.

[5] T. Stanev *et al.*, Phys. Rev. **D25**, 1291 (1985).

[6] M. Gyulassy at LBL is planning to look at this.

[7] M.L. Ter-Mikaelian, Dokl. Akad. Nauk. SSR **94**, 1033 (1954). For a discussion in English, see M.L. Ter-Mikaelian, *High Energy Electromagnetic Processes in Condensed Media*, John Wiley & Sons, 1972.

[8] W.R. Nelson, H. Yirayama and D.W.O.Rogers, SLAC-Report-265, Dec. 1985. Unfortunately, after such a nice discussion they did not include the effect in EGS.

[9] V.N. Baier and V.M Katkov, Sov. Phys. Doklady **17**, 1068 (1973); V.M. Katkov and V.M. Strakhovenko, Sov. J. Nucl. Phys. **25**, 660 (1977). Both papers find a logarithmic dependence on the magnetic field, with coefficients such that the earth's magnetic field (0.5 gauss) has of order 5-20% suppressing effect, depending on the energy.

[10] J.S. Bell, Nuclear Physics **8**, 613 (1958).

[11] In working out the integral in the first equation in section 3 of Bell's paper, a term $\delta(1-\cos\theta u)/t$ is omitted. Thanks to M. Gyulassy for pointing this out.

[12] P. Chen and S. Klein, unpublished work.

[13] E. Konishi *et al.*, J. Phys. G. **17**, 719 (1991). See also Ref. 6, and recent (1970's-1980's) proceedings of the Intl. Cosmic Ray Conf.

[14] A. Misaki, Fortschr. Phys. **38**, 413 (1990); J. G. Learned and T. Stanev, preprint HDC 1-91, submitted to the 3rd Venice Mtg. on Neutrino Telescopes, Venice, Italy, Feb., 1991.

[15] A. Bialas and T. Chmaj, Phys. Lett. **B133**, 241 (1983).

[16] S.J. Brodsky, G.T. Bodwin and G.P. Lepage, in *Proc. Intl. Conf. on Multiparticle Dynamics*, Volendam, 1982; S.J. Brodsky, in *Proc. of the Third Lake Louise Winter Institute on QCD*, 1988.

[17] P. Bordalo *et al.*, CERN preprints EP/87-67, EP/87-68.

[18] F.S. Dietrich *et al.*, Proposal to the SLAC EPAC, expected June, 1992.

[19] G. Raffelt and D. Seckel, Phys. Rev. Lett. **67**, 2605 (1991).

[20] S.C.Strausz *et al.*, in *Proc. 22nd Intl. Cosmic Ray. Conf.*, Dublin, Ireland, 11-23 Aug, 1991.

[21] P.H. Fowler *et al.*, Phil. Mag. **4**, 1030 (1959).

[22] A. Varfolomeev *et al.*, Sov. Phys. JETP **42**, 218 (1976).

[23] F.R. Arutyunyan, A.A. Nazarayan and A.A. Frangyan, Sov. Phys. JETP **35**, 1067 (1972).

[24] L. Jones in Proc. 22nd Intl. Cosmic Ray Conf. Dublin, Aug 11-23, 1991, Vol 4, pg. 237.

[25] Experiment D-31 Cu K-shell Impact Ionization by 5.1 GeV Electrons; W. E. Meyerhof, *et al.*, Phys. Rev. Lett. **68**, 2293 (1992).

[26] I. Kirkbride, in the SLAC Users Bulletin No. 97, Jan. - May 1984, pg. 10-11.

[27] P. Bosted and A. Rahbar, SLAC NPAS-TN-85-1, February, 1985.

[28] At slightly above 1 e^+/pulse.

Addendum to the Proposal for an Experiment to Study the Interference Between Multiple Scattering and Bremsstrahlung (The LPM Effect)

This proposal requires a low intensity e^+ (or e^-) beam. The beam design presented in the proposal requires dedicated use of the linac. Here, we wish to mention an alternative scheme that might allow the experiment to run parasitically, using photons generated by SLC beams hitting the sector 29 collimators. This scheme has just come to light recently, and will take some time to explore fully. In order to expedite matters, we are submitting the proposal as originally written now. If the parasitic beam proves workable, we would expect to use it instead of the dedicated beam requested in the proposal.

The photons generated in the sector 29 collimators continue downstream past the arcs, into a positron production target between the SLC splitter, 50B1, and the BSY pulse magnet string, PM1-5. Positrons produced in this target are then transported through the A-line into End Station A. Although a back of the envelope calculation yielded a potentially usable photon flux, a detailed EGS simulation remains to be completed. Also, there are a number of significant technical and practical objections to be overcome. If these objections are overcome, and parasitic beams become a reality, we will withdraw our request for dedicated beam time.

The parasitic beam will require a small number of modifications to the experimental apparatus, to deal with the shorter pulse and potentially larger beam size.

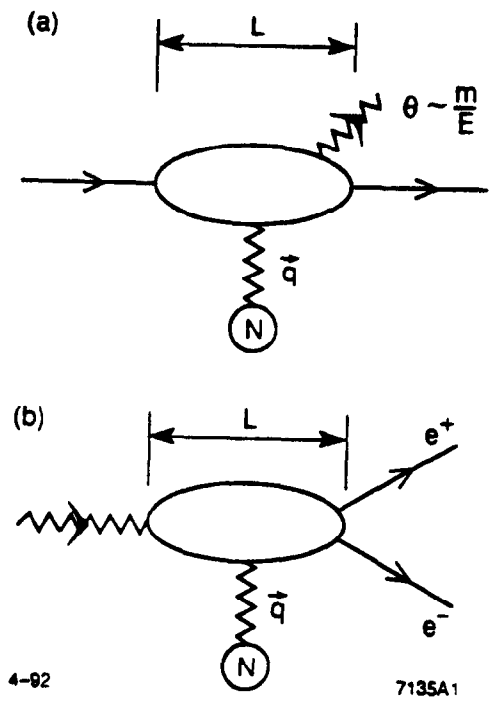

Figure 1. The Feynman diagrams for (a) bremsstrahlung and (b) pair creation. q is the momentum transfer between the nucleus and the electron, and L is the formation zone length, $c\gamma^2/\omega_\gamma$.

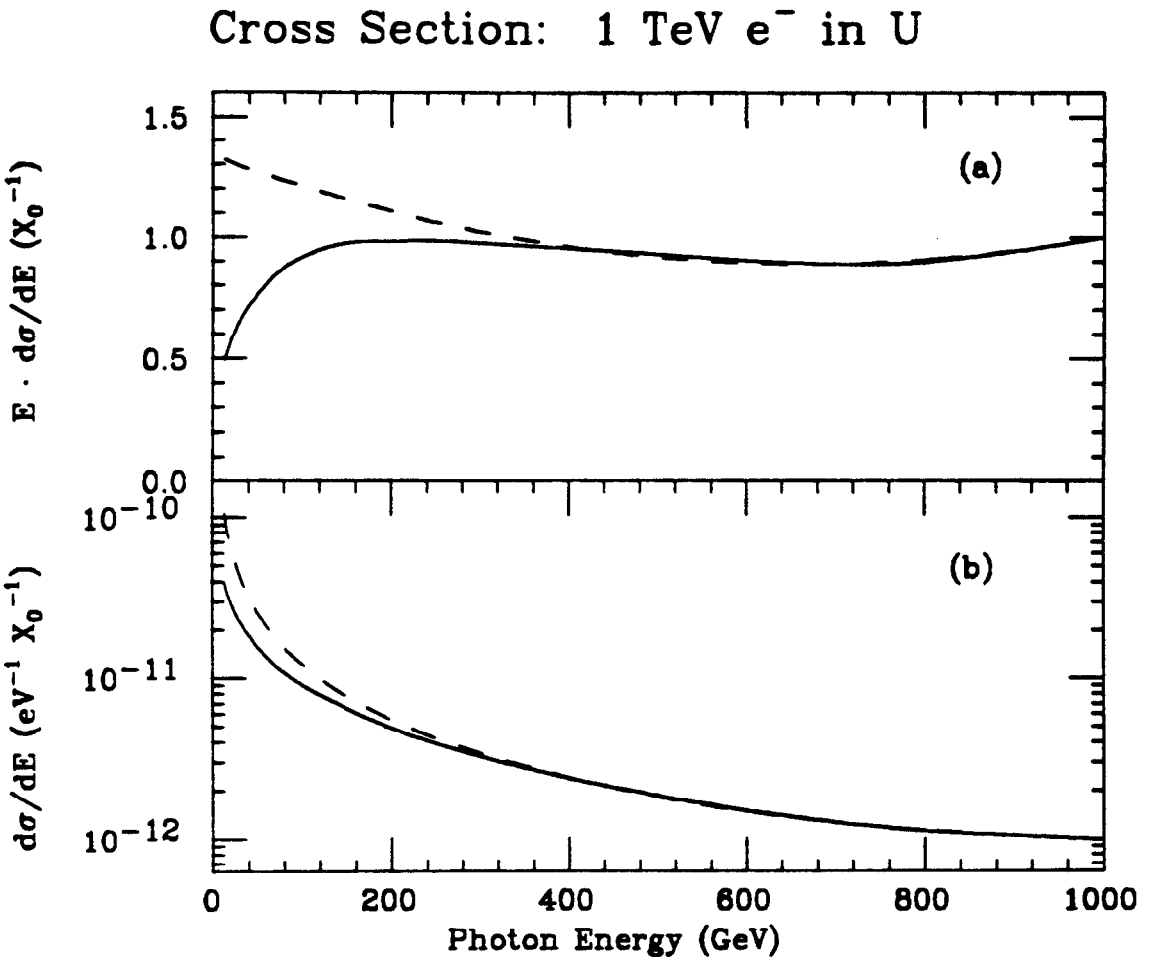

Figure 2. A comparison of the Bethe Heitler and LPM Cross sections for 1 TeV photons in uranium. 1 TeV is half E_{LPM} for uranium. (a) shows the energy weighted cross section, while (b) shows the total cross section.

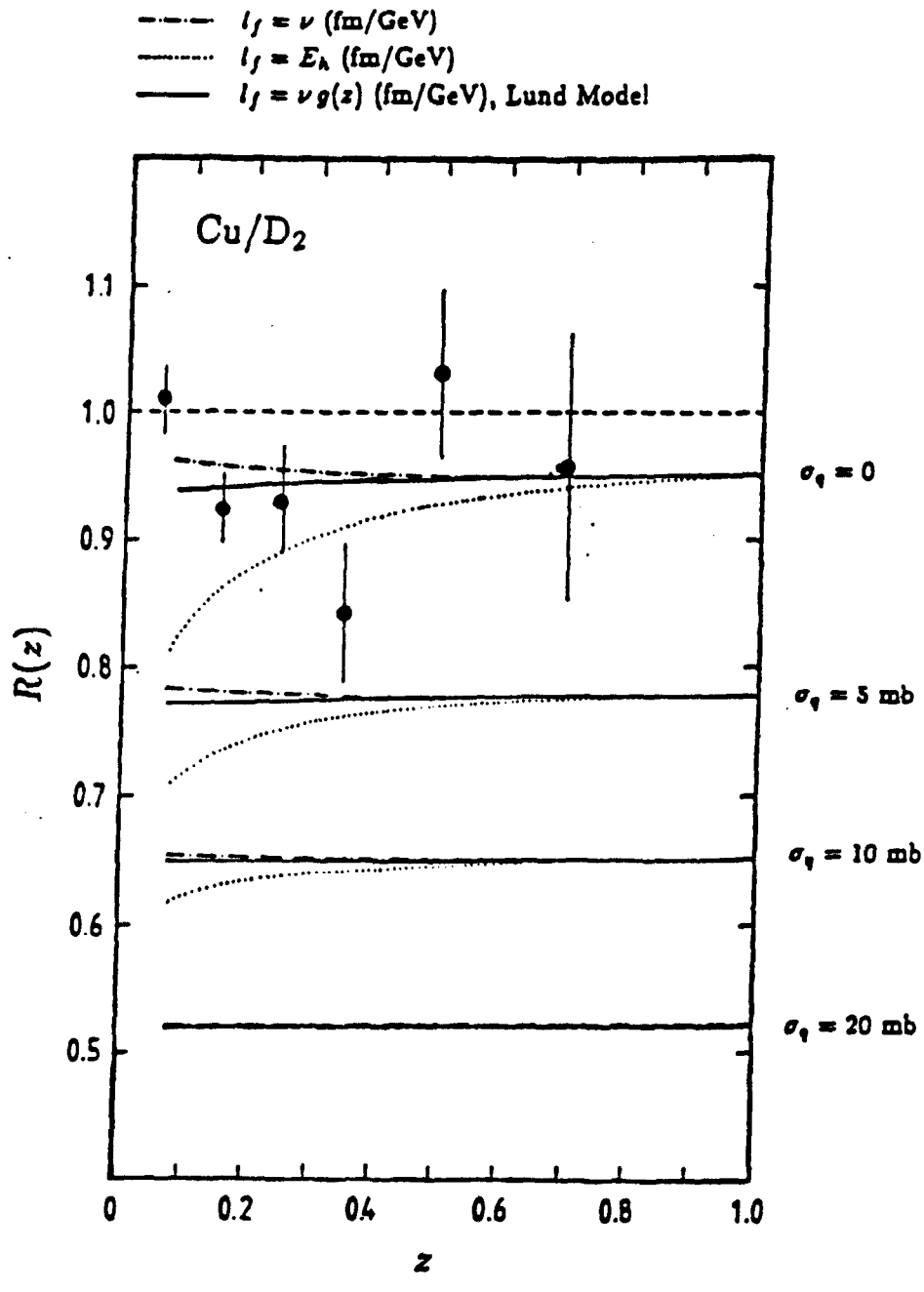

Figure 3. The nuclear transmission factor R for Cu compared to deuterium from the model of Bialas and Chmaj[15] using various formation lengths and quark nucleon cross sections.

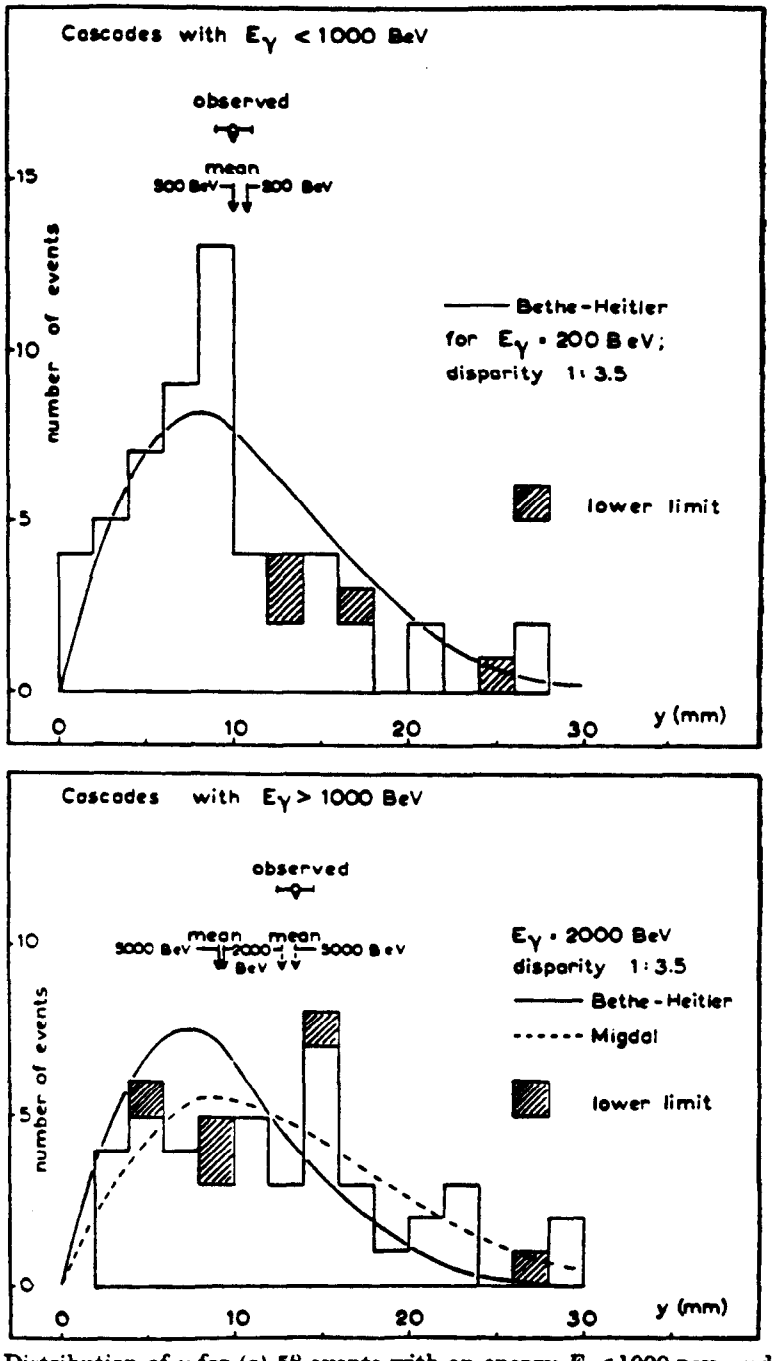

Distribution of y for (a) 58 events with an energy $E_\gamma < 1000$ Bev, and (b) 47 events with $E_\gamma > 1000$ Bev.

The error of one standard deviation is drawn to the observed mean value of y, and theoretical mean values are indicated for a few different primary energies.

Figure 4. The pair conversion depths measured by Fowler *et al.*. The 47 events in (b) are closer to the LPM (Migdal) curve.

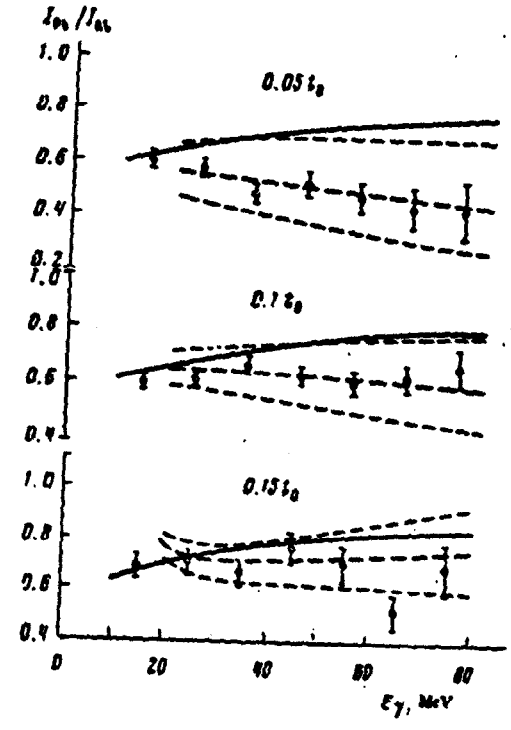

Figure 5. The ratio of bremsstrahlung spectra for (a) tungsten/carbon and (b) lead / aluminum, found by Varfolomeev *et al.*. The error bars are the data, the dotted line the LPM prediction, and the solid line the Bethe Heitler prediction. It is not entirely clear why they chose this method of data presentation.

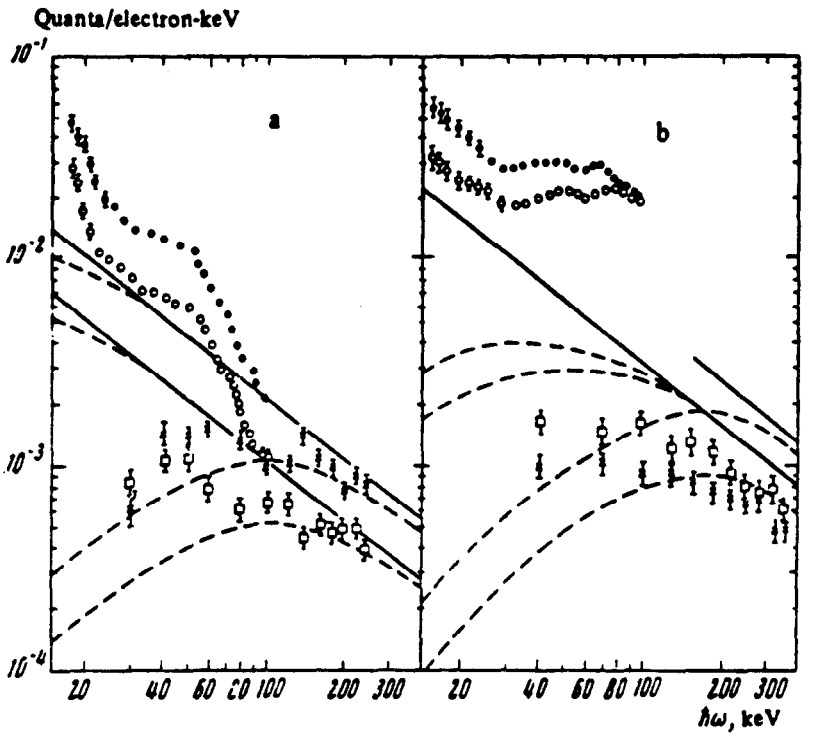

Figure 6. The dielectric suppression measured by Arutyunyan *et al.* for (a) glass and (b) aluminum. The solid lines are the BH curves, while the dashed include the density effect. In (a) the solid open and filled circles are from 250 MeV electrons into 7.3 and 3 cm thick targets respectively. In (b), the open and filled circles are from 450 MeV electrons into a 1.1 cm thick target and 600 MeV electrons into a 2.2 cm thick target. In (a) the crosses and squares are labelled 2.8 GeV electrons into 7.3 cm and 3 cm respectively. In (b), the energy remains 2.8 GeV, but with thicknesses of 1.1 and 2.2 cm. The solid lines are the BH (isolated atom) predictions for the two energies, while the dashed lines include dielectric effects.

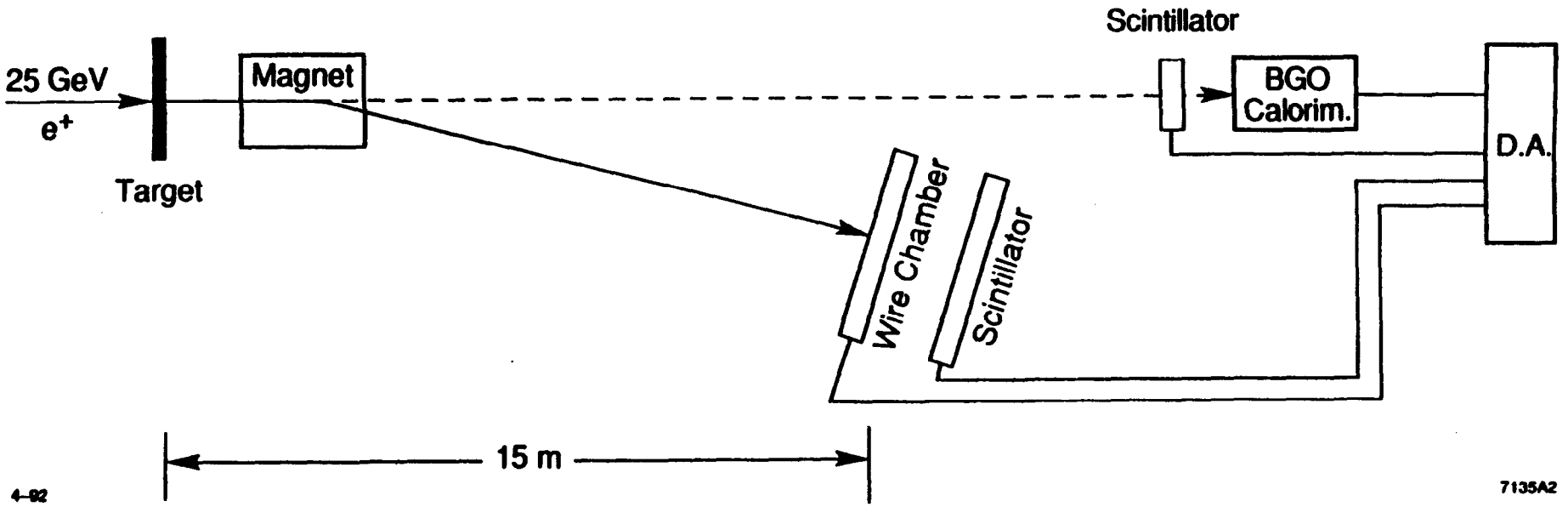

Figure 7. A block diagram of the proposed experiment. The various components are all described in the text.

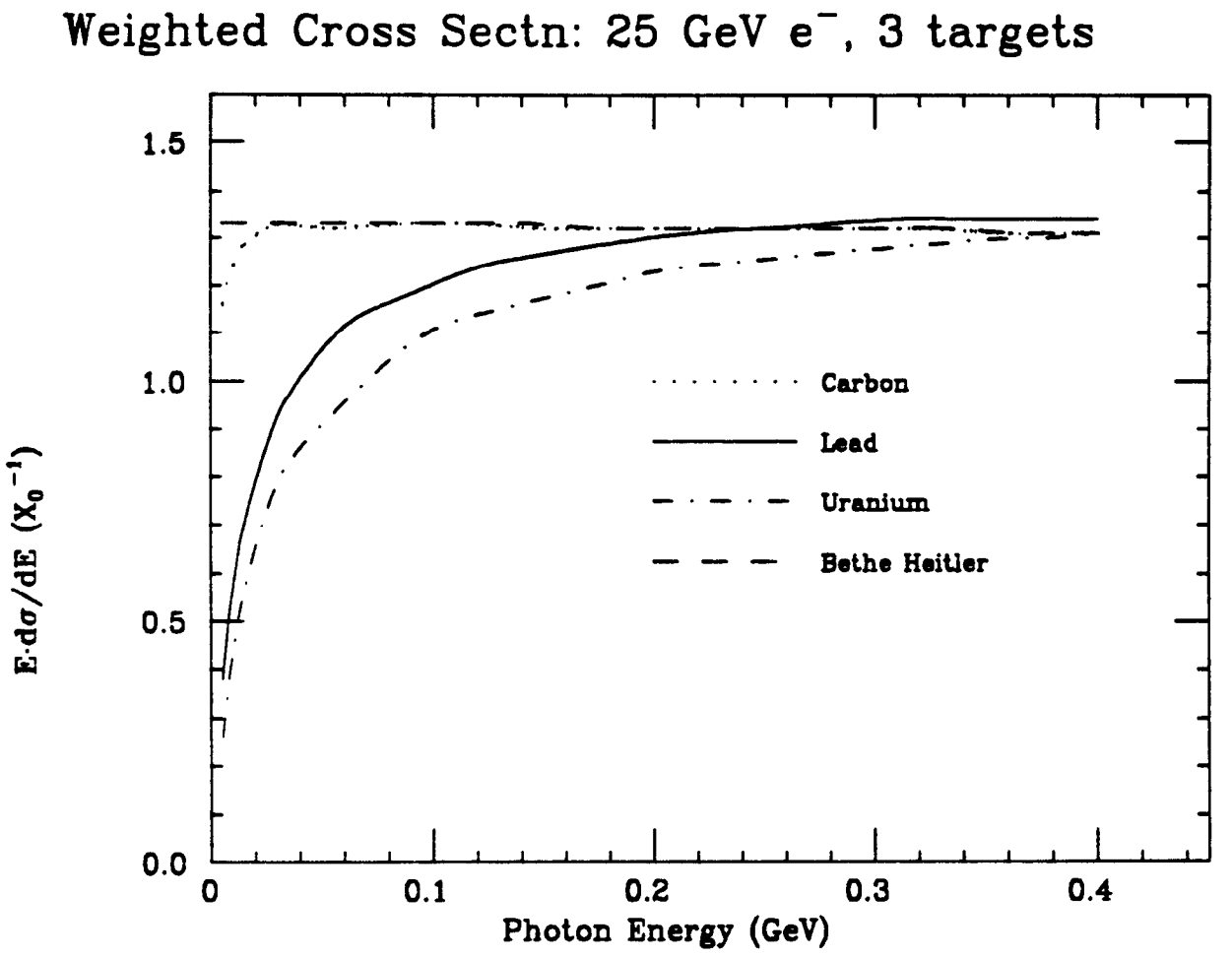

Figure 8. The expected cross sections for production of low energy photons from carbon (dashed line), lead (solid line) and uranium (dot-dashed line), and Bethe Heitler spectrum (dotted line). Tungsten lies very close to the uranium line.

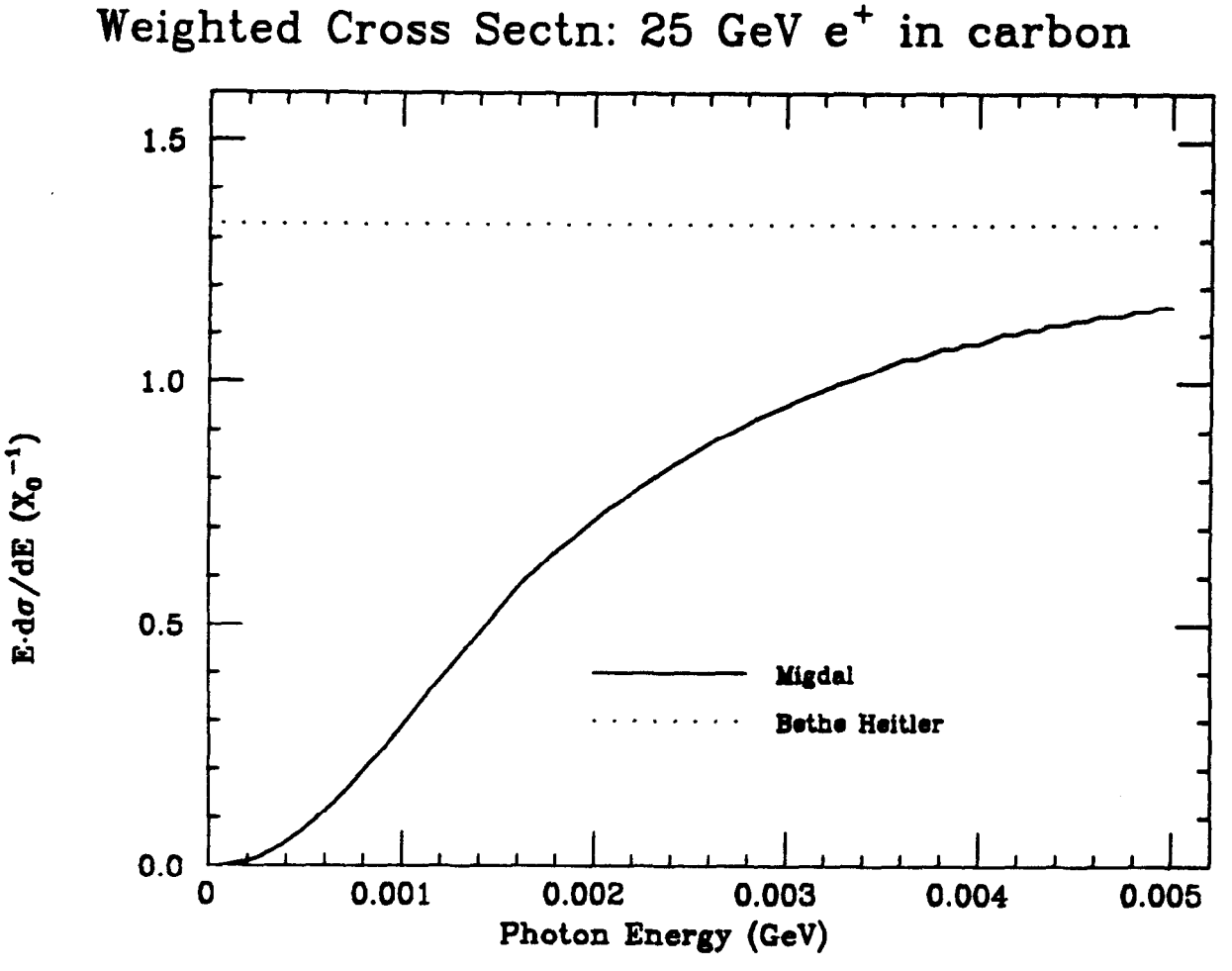

Figure 9. An exploded view of the weighted cross section for bremsstrahlung from carbon in the 0-5 MeV range, where the density effect turns on.

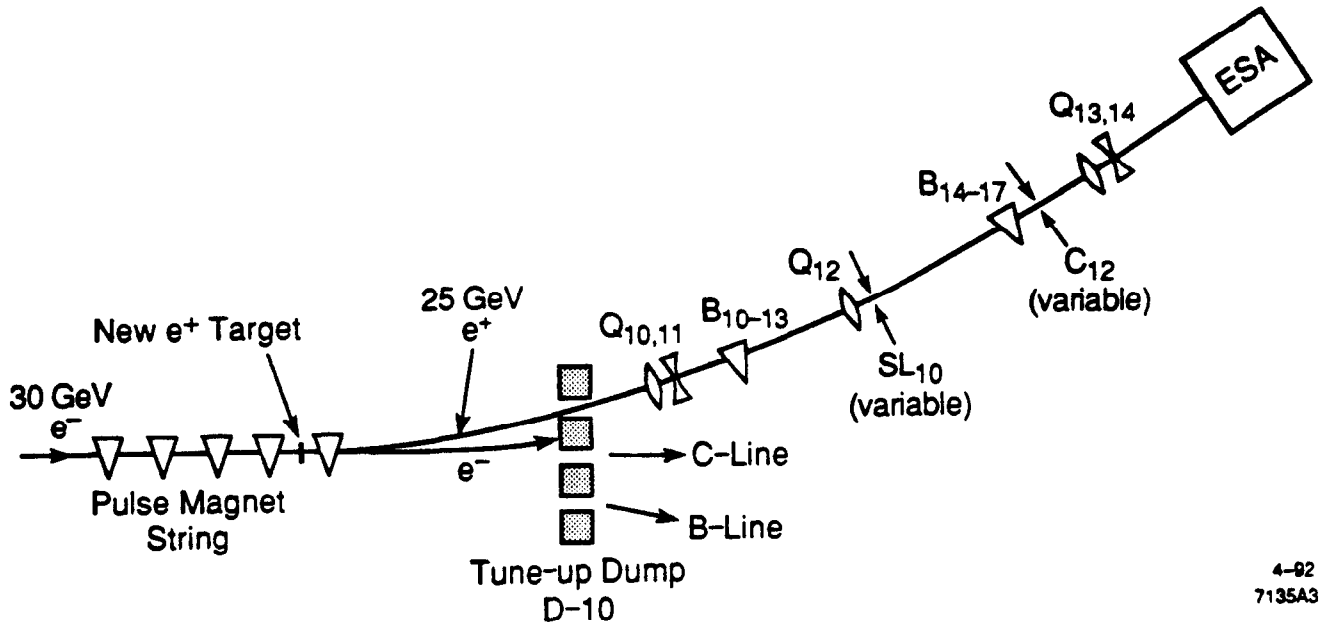

Figure 10. A schematic of the beam switchyard, showing the positron generation scheme. The only new component is the positron production target.

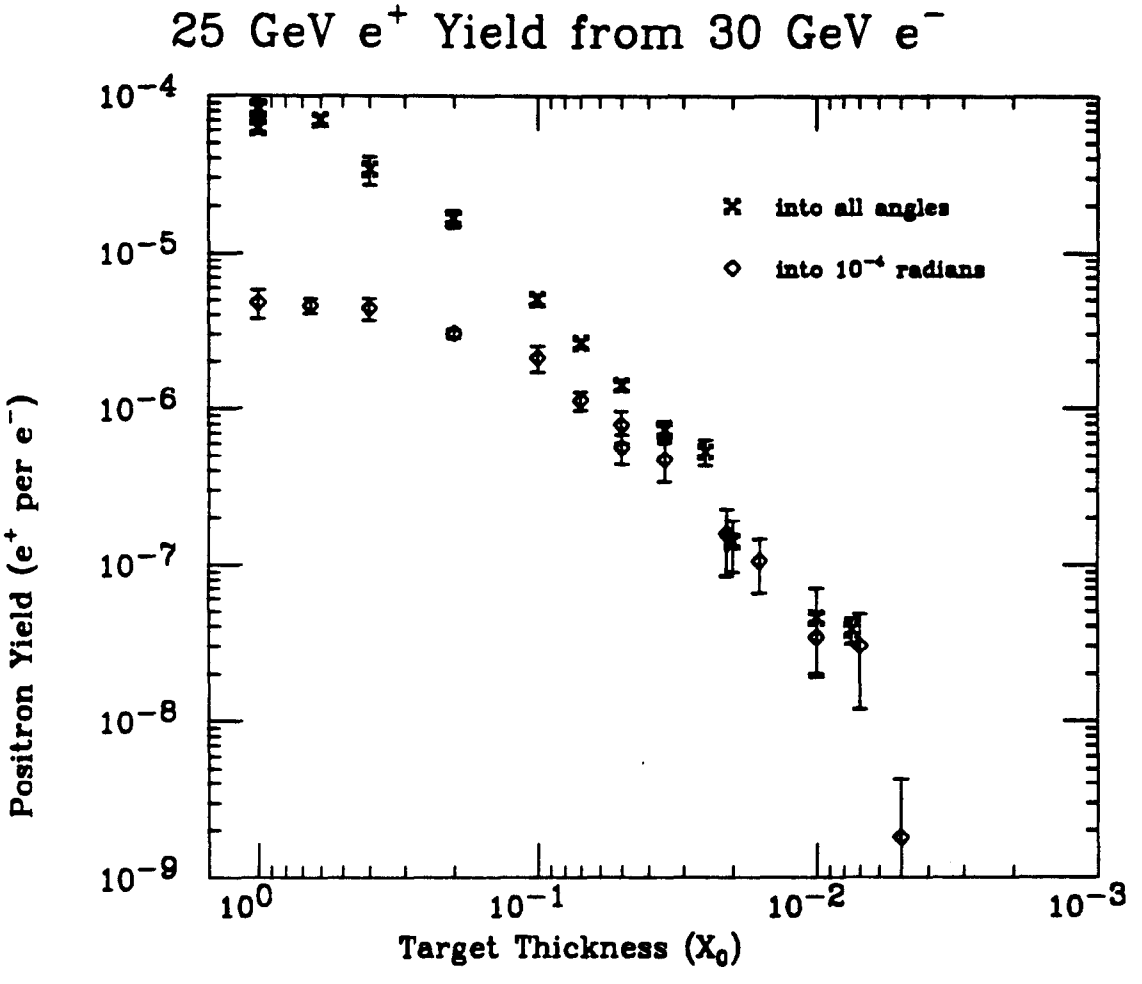

Figure 11. The expected yield (from EGS) of 25 GeV positrons from a a 30 GeV electron beam as a function of target thickness.

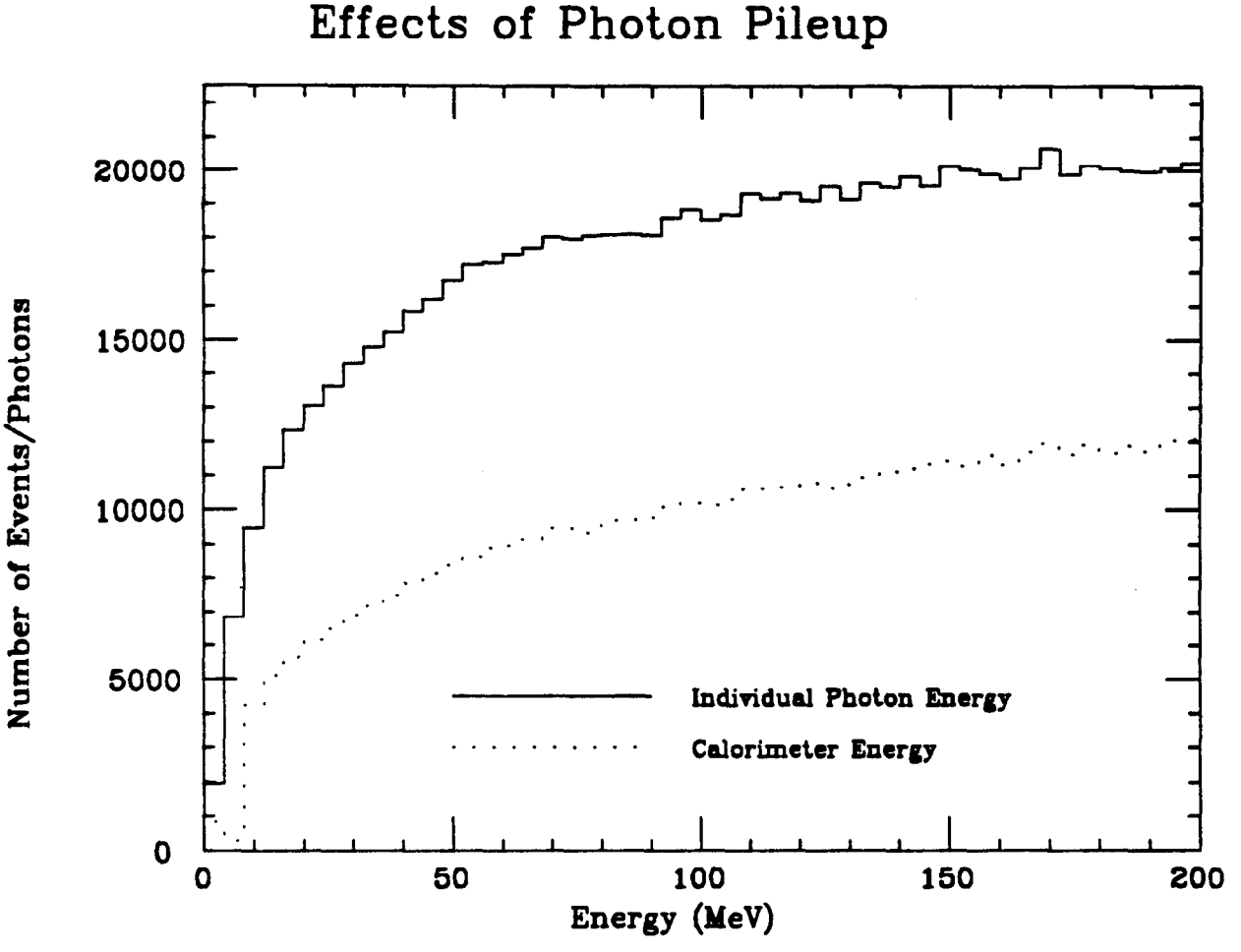

Figure 12. Histograms of Monte Carlo generated individual photon energies and total energy into the calorimeter, showing the effect of multiphoton pileup. Although multiphoton pileup reduces the rate of useful data collection, the shape of the curve is little affected. This plot is based on 4 million electrons, about 14 hours of data.

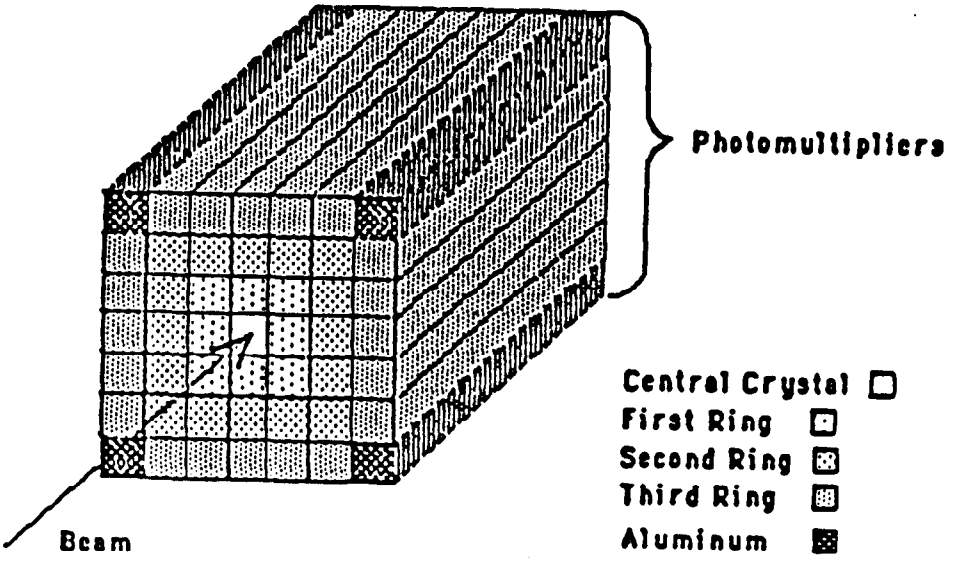

Figure 13. A drawing of the BGO calorimeter showing the 7 by 7 segmentation.

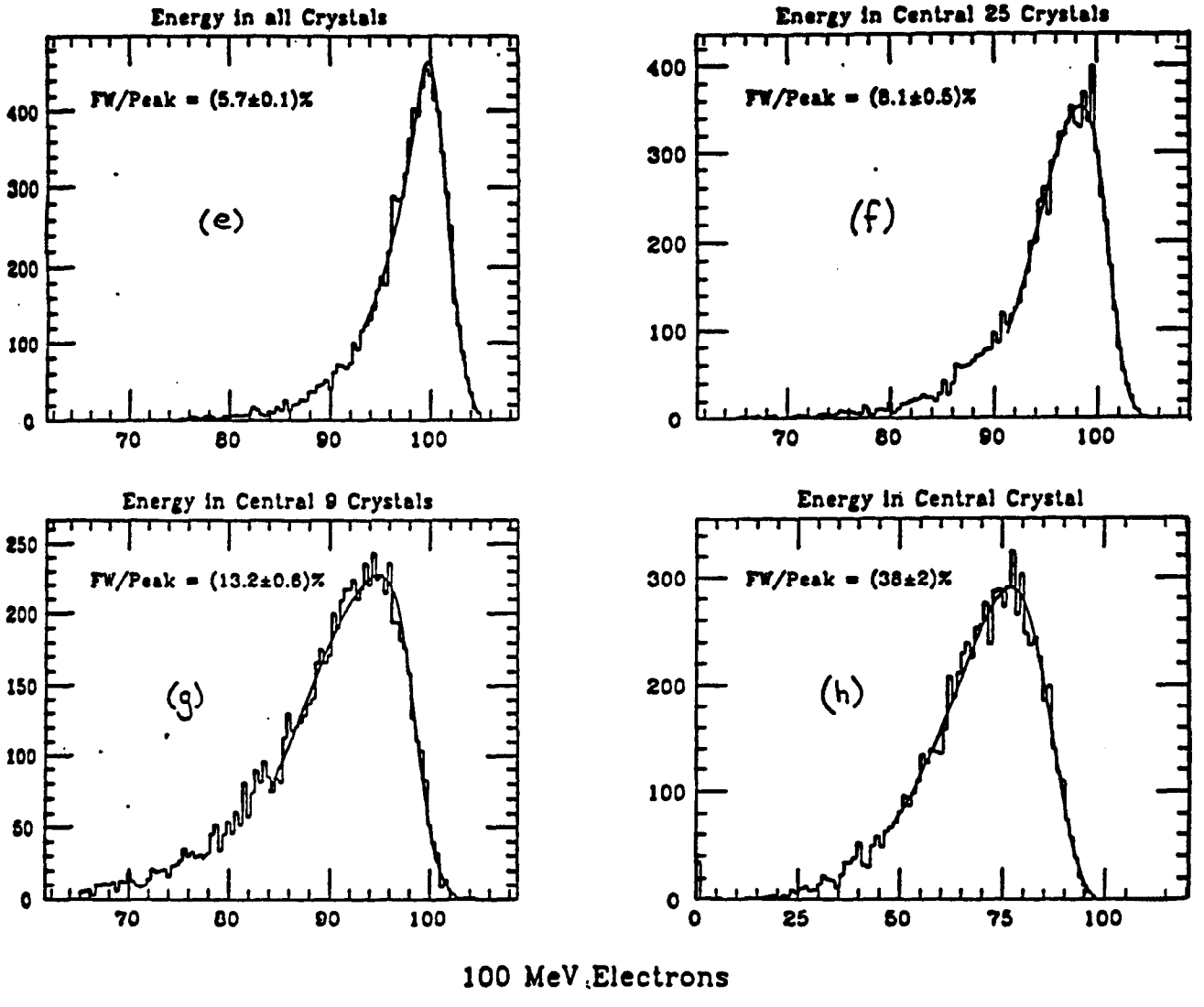

Figure 14. Energy spectra of 100 MeV electrons obtained with the BGO calorimeter summing different numbers of crystals.

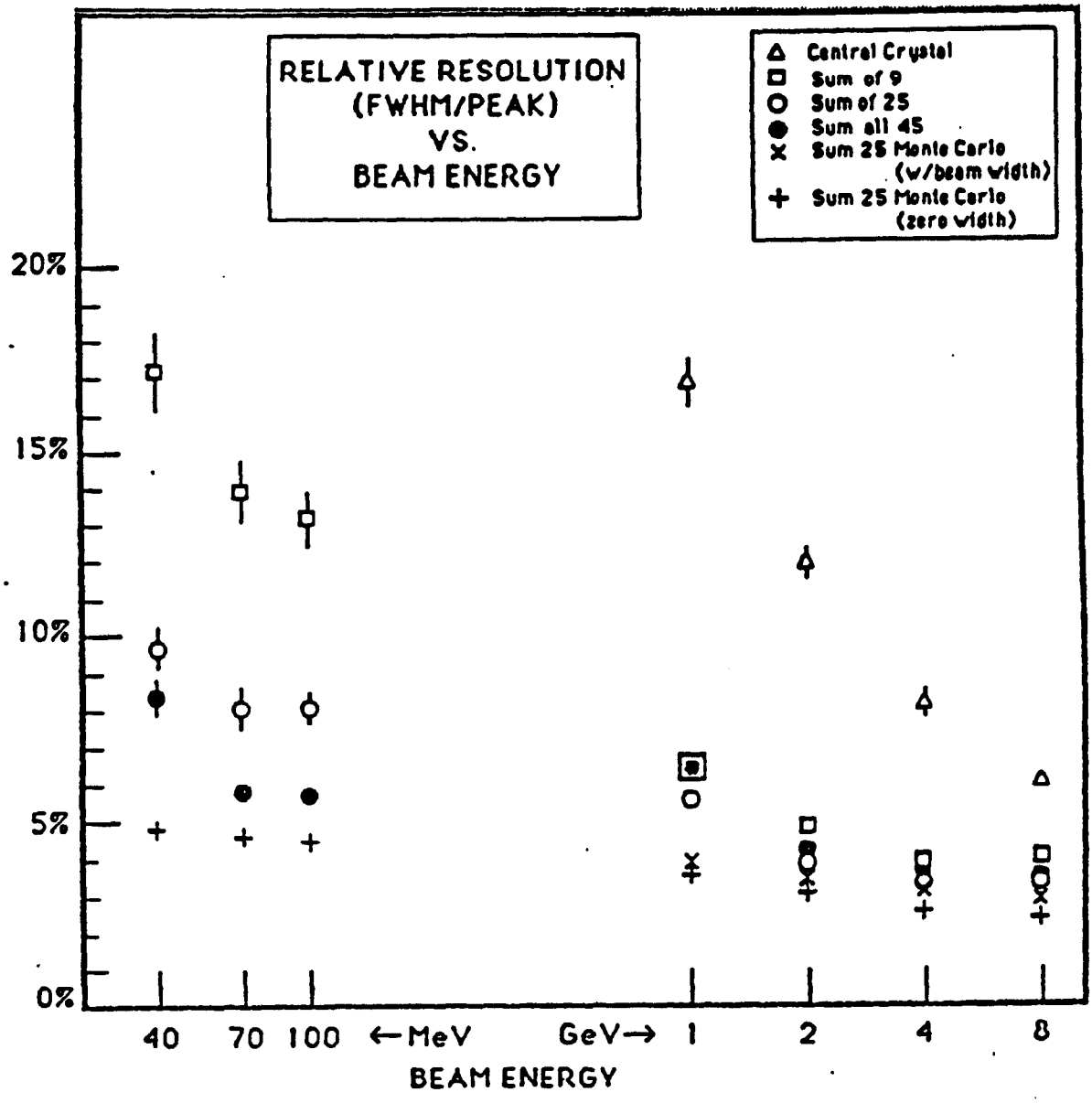

Figure 15. Energy resolution of the BGO calorimeter for various energy sums at energies from 40 MeV to 8 GeV. At high energies, the calorimeter is limited by leakage.

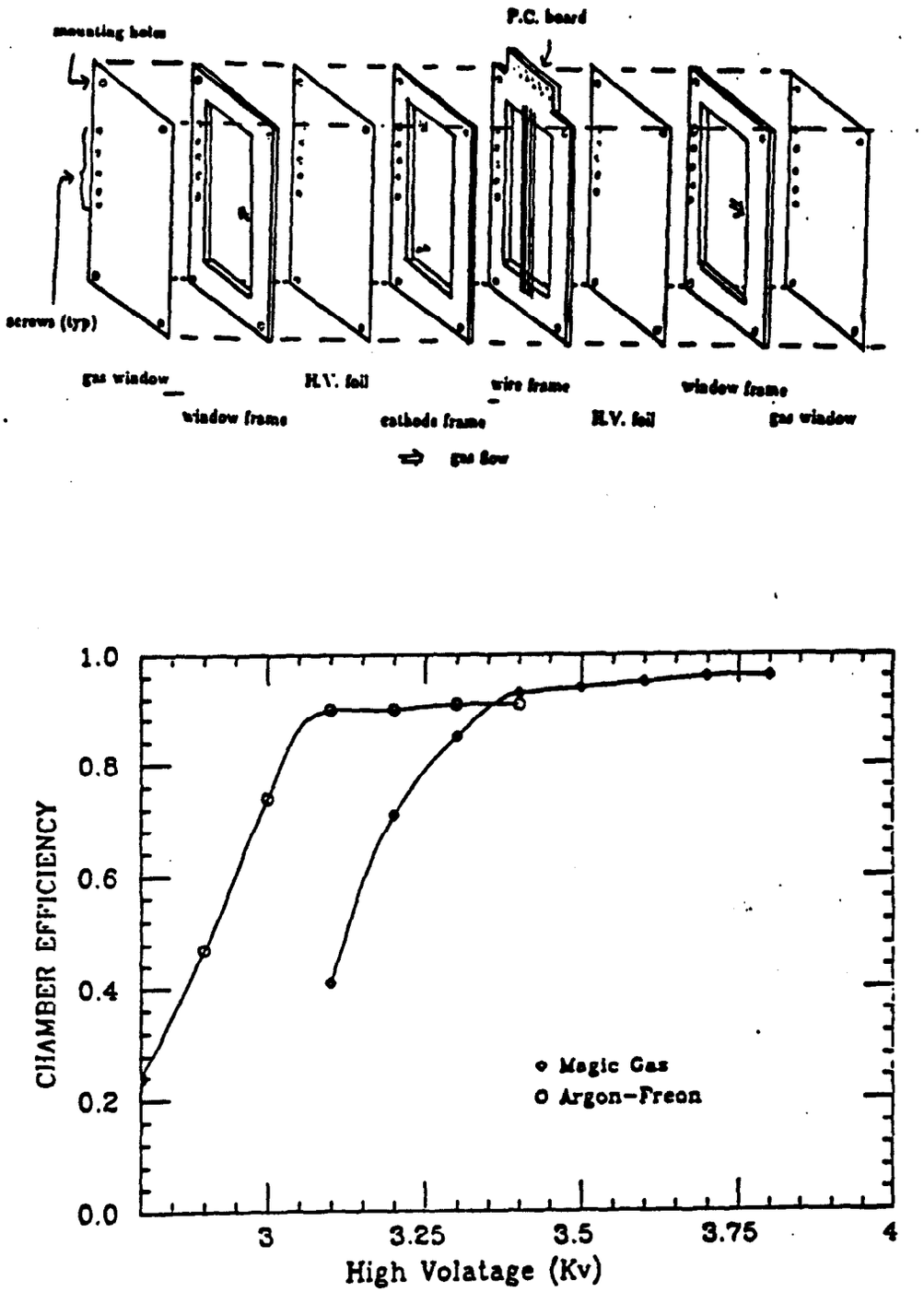

Figure 16. (a) Exploded view of one of the wire chambers and (b) chamber efficiency plateau.

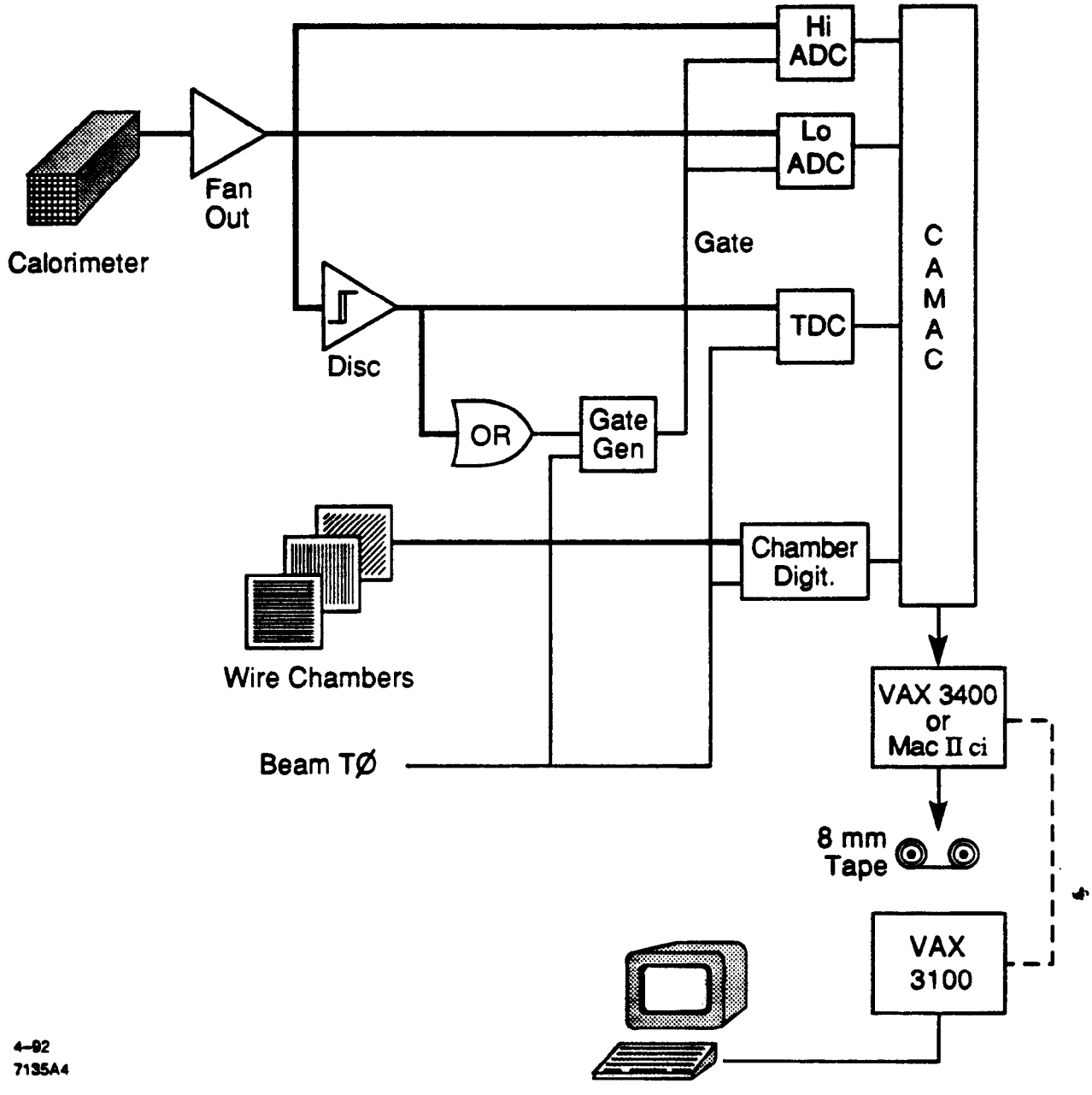

Figure 17. Block diagram of the electronics.